Article

Iron isotope fractionation during Fe(II) oxidation mediated by the oxygen-producing marine cyanobacterium Synechococcus PCC 7002

Elizabeth D Swanner, Timm Bayer, Wenfang Wu, Likai Hao, Martin Obst, Anneli Sundman, James Martin Byrne, F. Marc Michel, Ilka C Kleinhanns, Andreas Kappler, and Ronny Schoenberg

Environ. Sci. Technol., **Just Accepted Manuscript** • DOI: 10.1021/acs.est.6b05833 • Publication Date (Web): 12 Apr 2017

Iron isotope fractionation during Fe(II) oxidation mediated by the oxygen-producing marine cyanobacterium *Synechococcus* PCC 7002

Swanner, E.D.[1*], Bayer, T.[2], Wu, W.[2], Hao, L.[2], Obst, M.[3], Sundman, A.[2], Byrne, J. M.[2], Michel, F. M.[4], Kleinhanns, I. C.[2], Kappler A.[2], and R. Schoenberg[2].

[1]Iowa State University, Department of Geological & Atmospheric Sciences, Ames, IA USA.

[2]University of Tuebingen, Department of Geosciences, Tuebingen, Germany.

[3]University of Bayreuth, Bayreuth Center of Ecology and Environmental Research, Bayreuth, Germany.

[4]Department of Geosciences, Virginia Tech, Blacksburg, VA, USA.

*Corresponding author: Iowa State University, Department of Geological & Atmospheric Sciences, 2237 Osborn Drive, 253 Science I, Ames, IA 50011-1027, phone: (515) 294-5826, fax: (515) 294-6049, email: eswanner@iastate.edu

Abstract

In this study, we couple iron isotope analysis to microscopic and mineralogical investigation of iron speciation during circumneutral Fe(II) oxidation and Fe(III) precipitation with photosynthetically produced oxygen. In the presence of the cyanobacterium *Synechococcus* PCC 7002, aqueous Fe(II) ($Fe(II)_{aq}$) is oxidized and precipitated as amorphous Fe(III) oxyhydroxide minerals (iron precipitates, Fe_{ppt}), with distinct isotopic fractionation ($\varepsilon^{56}Fe$) values determined from fitting the $\delta^{56}Fe(II)_{aq}$ (1.79 and 2.15 ‰) and the $\delta^{56}Fe_{ppt}$ (2.44 and 2.98 ‰) data trends from two replicate experiments. Additional Fe(II) and Fe(III) phases were detected using microscopy and chemical extractions, and likely represent Fe(II) and Fe(III) sorbed to minerals and cells. The iron desorbed with sodium acetate (Fe_{NaAc}) yielded heavier $\delta^{56}Fe$ compositions than $Fe(II)_{aq}$. Modeling of the fractionation during Fe(III) sorption to cells and Fe(II) sorption to $Fe_{ppt,}$ combined with equilibration of sorbed iron and with $Fe(II)_{aq}$ using published fractionation factors are consistent with our resulting $\delta^{56}Fe_{NaAc}$. The $\delta^{56}Fe_{ppt}$ data trend is inconsistent with complete equilibrium exchange with $Fe(II)_{aq.}$ Because of this and our detection of microbially-excreted organics (e.g. exopolysaccharides) coating Fe_{ppt} in our microscopic analysis, we suggest that electron and atom exchange is partially suppressed in this system by biologically-produced organics. These results indicate that cyanobacteria influence the fate and composition of iron in sunlit environments via their role in Fe(II) oxidation through O_2 production, the capacity of their cell surfaces to sorb iron, and via the interaction of secreted organics with Fe(III) minerals.

Introduction

Fe(II)-oxidizing bacteria (FeOB) gain energy from the chemical oxidation of Fe(II) coupled to reduction of oxygen or nitrate, or using light energy coupled to reduction of CO_2, e.g. anoxygenic photosynthesis[1]. At the near neutral pH of many surface waters, the oxidation of Fe(II) is spontaneous and rapid in the presence of dissolved oxygen. For that reason, cyanobacteria, which generate oxygen as a result of oxygenic photosynthesis, can act as indirect Fe(II)-oxidizing bacteria where anoxic and Fe(II)-containing deep waters upwell to sunlit surface environments.

The contribution of cyanobacteria to Fe(II) oxidation has been quantitatively addressed in Fe(II)-rich hot spring environments[2], and in benthic photosynthetic communities living at the sediment-water interface[3]. Although the modern oceans are predominantly oxygenated to great depths, promoting the speciation of iron as ferric [Fe(III)] rather than ferrous [Fe(II)], Fe(II) may be increasingly mobilized out of sediments[4-7] and stabilized in the marine water column due to expanding low-oxygen conditions in so-called oxygen minimum zones (OMZ)[8]. Where OMZ intersect with the photic zone, Fe(II) oxidation by planktonic oxygen-producing cyanobacteria could contribute to the marine iron cycle. Furthermore, anoxic and Fe(II)-rich bottom waters are a pervasive feature of oceans in the Precambrian Era [before about 500 Million years (My) ago][9, 10] at a time when oxygen was building up in the surface oceans as a result of cyanobacteria and other oxygenic phototrophs[11-13]. Therefore, redox interfaces between anoxic and Fe(II)-containing waters and photosynthetically-produced oxygen were likely common throughout much of Earth's history.

Iron redox processes fractionate the naturally occurring isotopes of iron dependent on their mass (e.g. ^{54}Fe, ^{56}Fe, ^{57}Fe, and ^{58}Fe), such that the quantitative contribution of biotic and abiotic iron cycling at the Earth's surface may be recorded in sediments composed of iron-rich minerals[14, 15]. Due to the large fractionations between Fe(II) and Fe(III) species[16], Fe(II) oxidation generally produces a solid iron phase that is enriched in heavy isotopes of iron relative to aqueous Fe(II), regardless of the mechanism of oxidation[17]. This makes it difficult to parse the contribution of enzymatic Fe(II)-oxidizing bacteria from abiotic Fe(II) oxidation, not to mention indirect Fe(II) oxidation by oxygen-producing cyanobacteria by using iron isotopes. However, subtle differences in the mechanism of oxidation and precipitation, and in the characteristics of the iron minerals or phases (e.g. mineralogy, particle size, or presence of impurities) formed can influence the overall fractionation between aqueous Fe(II) and iron minerals[18]. Furthermore, the role of cyanobacteria in direct or indirect redox cycling of iron at the cell surface is increasingly recognized[19-22], and may be associated with distinct isotope fractionation[23]. Therefore, detailed mechanistic studies of iron isotope fractionation during different pathways of Fe(II) oxidation are warranted, and may help to define isotopic, mineralogical, or microscopic signatures associated with certain biological processes.

Furthermore, the isotopic composition of iron minerals is known to be modified by electron and atom exchange between aqueous Fe(II) and Fe(III) (oxyhdr)oxide minerals[24-26]. These processes have been most effectively characterized under reducing conditions, when a supply of aqueous Fe(II) is produced by, for instance, microbial Fe(III) reduction[27, 28]. However, at Fe(II)-O_2

interfaces with a flux of aqueous Fe(II), electron and atom-exchange could also occur on newly-formed Fe(III) (oxyhydr)oxide minerals[29]. Although the effect of some organics, as well as Si and low pH on blocking electron and atom exchange have been investigated[30-32], the effect of cell surfaces and microbially-produced organics on this reaction and via blocking sites on Fe(III) minerals, particularly in an oxidizing system, are not known.

In this contribution, we tracked the iron isotope composition of different pools of iron during Fe(II) oxidation by the marine planktonic cyanobacterium *Synechococcus* PCC 7002. Several prior studies have characterized the interaction of this oxygen-producing strain with Fe(II)[33, 34], which gives us a body of work to aid in interpreting the nature of different iron phases in the system, and their mechanism of transformation. Additional microscopy and mineral characterization in this study are used to build the picture of how iron is processed during indirect Fe(II) oxidation resulting from oxygenic photosynthesis. The results have implications for understanding the reactivity of iron minerals as well as identifying isotopic signatures associated with biological activity.

Experimental

Bacterial Growth Medium

Synechococcus PCC 7002 was routinely cultivated on pH 6.8 Marine Phototroph (MP) medium[18, 33, 35] containing 6 mg L^{-1} ferric ammonium citrate as the Fe(III) source at 24°C under an irradiance of 12.8 μmol photons m^{-1} s^{-1} from a standard

105 40W tungsten light bulb as measured by a Li-250A light probe (Li-cor, Inc.). For
106 Fe(II) oxidation experiments, MP medium was made without ferric ammonium
107 citrate. Fe(II) amendments were added from a sterile, anoxic $FeCl_2$ stock solution
108 and the medium was filtered twice through a 0.22 μm filter in an anoxic glovebox
109 (100% N_2), separated by 48 hour incubations at 4°C to ensure that all Fe(II)
110 precipitated as carbonate and phosphate minerals with growth media components
111 were removed[18]. The final Fe(II) concentration in the medium after filtration was 2
112 mM as measured by the spectrophotometric Ferrozine assay. A log-phase culture of
113 *Synechococcus* PCC 7002 grown with ferric ammonium citrate was degassed for 5
114 minutes with sterile N_2:CO_2 (90%:10%), and inoculated into the 2 mM Fe(II)-
115 containing medium to a final concentration of $5x10^6$ cells mL^{-1} [33]. Growth conditions
116 were as above.
117 Glass media bottles were acid washed in 1 M HCl for 24 h, then soaked in fresh
118 ultrapure water (resistivity of 18.2 MΩ cm^{-1}) for two successive 24 h treatments
119 before use. Experiments utilized 100 mL bottles filled to 80 mL with growth
120 medium. All anoxic bottles were closed with butyl rubber stoppers that had been
121 washed in 1N HCl for 24 h, then thrice boiled in ultrapure water.
122 This concentration of 2 mM Fe(II) was chosen for experiments because a freshly
123 inoculated culture of *Synechococcus* PCC 7002 took about ten days to oxidize this,
124 during which time we could sample sufficiently often to have resolution on the
125 evolution of the isotopic composition of different iron pools. Despite the fact that
126 this strain grows more slowly at 2 mM Fe(II) than at lower Fe(II) concentrations,
127 due to Fe(II) toxicity[33, 34], sufficient growth did occur to fully oxidize all Fe(II).

Although this concentration is at the upper end of Fe(II) concentrations in modern sunlit environments[36, 37], it is within the range documented for environments where cyanobacteria have been documented as having a role in Fe(II) oxidation[2, 3].

Iron species separation, Fe(II) and total iron concentration determination

During Fe(II) oxidation, which lasted about 10 days, volumes of 2 mL were repeatedly removed with a syringe from the bottles of two contemporaneous replicate experiments (samples 1 and 2) in an anoxic glovebox. Before extracting, the bottles were shaken to yield a homogenous slurry of iron precipitates. The aliquots were subsequently centrifuged for 10 minutes at 16,000 g, and the supernatants were filtered through a nylon 0.22 μm centrifuge tube filter (Costar Spin-X, Corning, International) to yield particle-free aqueous Fe(II), henceforth $Fe(II)_{aq}$. The solids were washed with anoxic ultrapure water to remove any loosely bound iron. A second wash utilized anoxic 0.5 M sodium acetate (adjusted to pH 4.85 using acetic acid) to recover sorbed iron (Fe_{NaAc}) from the solids (24 h incubation in the dark)[29, 38]. The remaining solids were considered the precipitated fraction (Fe_{ppt}).

The concentrations of Fe(II) and total iron in the four different iron fractions were measured with the ferrozine assay[39]. The Fe(II) in the $Fe(II)_{aq}$, water wash, and in Fe_{NaAc} was stabilized in a final concentration of anoxic 1 M HCl prior to measurements. The Fe_{ppt} was dissolved in 6 N anoxic HCl before analysis. Fe(III)

was determined as the difference between Fe(II) measurement and total iron measurements (after reduction of iron by hydroxylamine hydrochloride).

Fe isotope analysis

Purification of the $Fe(II)_{aq}$, Fe_{NaAc}, and Fe_{ppt} fractions was performed in positively pressured clean laboratories of the Isotope Geochemistry group at the University of Tuebingen under conditions and with reagents that have previously been described[40]. The concentrations of iron in the water washes of Fe_{ppt} were below the detection limit of the ferrozine assay (<0.01 mM, 0.56 μg mL^{-1}), and so these samples were not purified. Sample aliquots of the separated iron fractions containing 5 μg of iron were purified for iron isotope measurements using anion exchange chromatography according to prior methodology[40]. An adequate amount of ^{57}Fe-^{58}Fe double spike was added to the samples prior to Fe purification to ensure accurate correction of the instrumental mass bias and possible Fe isotope fractionation during anion chromatography caused by the organic matrix of the samples[18]. Iron isotope analyses were performed on the ThermoFisher Scientific NeptunePlus multi-collector inductively coupled plasma mass spectrometer (MC-ICP-MS) of the Isotope Geochemistry group of the University of Tuebingen. Polyatomic interferences, such as $^{40}Ar^{14}N^+$ on $^{54}Fe^+$ or $^{40}Ar^{16}O^+$ on $^{56}Fe^+$ were resolved using the high mass-resolution mode (16 μm slit). The four iron isotope beams were simultaneously detected with 90 integration cycles at 8 seconds each during the runs. Background corrections for sample signals were based on on-peak-zero measurements on the pure analyte solution (0.3 M HNO_3) run before and after

each sample. Iron isotope data are reported relative to the isotopically certified international reference material IRMM-014 (Institute for Reference Materials and Measurements in Gent, Belgium) using the δ-notation:

$$\delta^{56}Fe = [(^{56}Fe/^{54}Fe)_{sample} / (^{56}Fe/^{54}Fe)_{IRMM\text{-}014} - 1] \times 1000$$

The results are reported in units of per mil (‰). The reproducibility of the double-spike measuring method as determined by repeated $\delta^{56}Fe$ measurements of the IRMM-014 reference material in between sample runs was 0.00 ± 0.032 ‰ (2SD; n = 18). Interspersed measurements of our in-house iron standard, HanFe, yielded $\delta^{56}Fe$ = 0.282 ± 0.039 ‰ (2SD; n = 12), which is in excellent agreement with previously published values of 0.28 ± 0.05 ‰ (2SD; n = 19)[41] and 0.279 ± 0.030 ‰ (2SD; n = 5)[18].

Rayleigh fits of the isotopic $\delta^{56}Fe(II)_{aq}$ and $\delta^{56}Fe_{ppt}$ at different fractions (f) of Fe(II) remaining were utilized to determine the isotopic enrichment factor ($\alpha^{56}Fe$) using the following equations:

$$\delta^{56}Fe(II)_{aq} = (\delta^{56}Fe(II)_{aq\text{-}0}+1000)\times f^{\alpha-1}-1000 \quad (1)$$

$$\delta^{56}Fe_{ppt} = (\delta^{56}Fe_{aq\text{-}0}+1000)\times[(1 - f^{\alpha})/(1-f)] -1000 \quad (2)$$

$\delta^{56}Fe(II)_{aq\text{-}0}$ indicates the $\delta^{56}Fe(II)_{aq}$ at the beginning of the experiment. The isotopic fractionation $\varepsilon^{56}Fe$ (‰) is related to α by the equation:

$$\varepsilon^{56}Fe = 1000 \times ln\ \alpha^{56}Fe \quad (1)$$

The fitting parameters were determined by minimizing the sum of chi^2 values. Data were also fit by linear regression, with slope and intercept determined by minimizing the sum of chi^2 values.

194 **Mineral Characterization**

195 High energy synchrotron X-ray scattering experiments were performed on
196 the solid, dry products of Fe(II) oxidation by *Synechococcus* PCC 7002 at the
197 Advanced Photon Source at Argonne National Laboratory, Beamline 11-ID-B. The
198 solids were collected from a culture grown with ca. 5 mM Fe(II), freeze-dried, and
199 washed three times with Millipore water to remove excess salt. Data collection and
200 analysis protocols were previously described[18]. Additional mineral characterization
201 methods and results are described in the **Supplementary Information**.

202

203 **Confocal Laser Scanning Microscopy**

204

205 Cells of *Synechococcus* PCC 7002 were grown under similar conditions as
206 described above until the initial ca. 0.5 mM Fe(II) had been oxidized. The cell-
207 mineral aggregates were imaged by confocal laser scanning microscopy (CLSM;
208 Leica SPE, Mannheim, Germany). A 635 nm laser was used for excitation
209 autofluorescence of *Synechococcus* PCC 7002, with a maximum emission peak at 660
210 nm (detected range of emission 640-700 nm). The Fe(III) minerals were visualized
211 using the reflection signal of the 488 nm laser. Several lectin-Alexa dye conjugates
212 were screened in order to optimize visualization of exopolysaccharides (EPS)
213 without overlap with the autofluorescence emission maximum of the pigments of
214 *Synechococcus* PCC 7002 (660 nm). SBA-Alexa 488 (maximum emission peak at 520
215 nm) was chosen because SBA bound to the EPS in higher amounts, resulting in
216 brighter fluorescence than the other lectins screened [Wheat Germ Agglutinin Alexa

Fluor 555 Conjugate (WGA-555) and Lectin PNA from *Arachis hypogaea* (peanut), Alex Fluor 568 Conjugate (PNA-568)]. Brighter fluorescence at lower laser power was observed with SBA-488, which binds terminal α- and β-N-acetylgalactosamine and galactopyranosyl residues, compared to WGA-555 and PNA-568, which are specific to sialic acid and *N*-acetylglucosaminyl residues, and terminal β-galactose, respectively.

A turn-on type selective probe for fluorescent labeling of dissolved, sorbed, or ligand-bound Fe(III)[42, 43], was previously used to visualize the relationship of Fe(III) *Synechococcus* PCC 7002 cells and minerals from this same incubation[34]. Because of spectral overlap, the lectin and Fe(III)-binding probe could not be combined in a single experiment here, and therefore we compare new results to prior data[34]. The Auto-Quant™ deconvolution algorithm implemented in the LEICA LAS AF software was applied to blind deconvolute the 3D image stacks[44]. The spatial relationships of species detected using fluorescence dyes and cell autofluorescence in CLSM image stacks were analyzed using ScatterJ[45], a plugin for correlation analysis of species-specific maps for use in IMAGEJ and Fiji[46].

Results & Discussion

Fractionation patterns during Fe(II) oxidation and Fe(III) precipitation

The $\delta^{56}Fe(II)_{aq}$ values from two replicated experiments evolved from an initial value near 0 ‰ to lighter values during oxidation (**Table 1, Figure 1**). The $Fe(II)_{aq}$ fraction, measured after the sample was centrifuged and filtered, consisted of only Fe(II). All iron concentration and speciation data (measured by ferrozine) is

239 reported in **Supplementary Table 1**. The first Fe_{ppt} samples analyzed, at about 40%
240 Fe(II) oxidized, had $\delta^{56}Fe_{ppt}$ of about 2 ‰, trending toward 0 ‰ at 100% Fe(II)
241 oxidized. The speciation of Fe_{ppt}, which was measured after washing with water and
242 sodium acetate, consisted of predominantly Fe(III), with generally <10% Fe(II). Iron
243 in the water wash of the precipitates was below the detection limit of the ferrozine
244 assay (<0.01 mM, 0.56 μg mL^{-1}). Therefore, the iron isotope composition of the
245 water washes was not analyzed. The sodium acetate wash removed sorbed iron,
246 which contained both Fe(II) and Fe(III). The Fe_{NaAc} fraction represented 10-20% of
247 total iron in the system after Fe_{ppt} began to form. The Fe_{NaAc} had an intermediate
248 isotopic composition between $Fe(II)_{aq}$ and Fe_{ppt}, but was variable and generally
249 lighter than 0 ‰.

250 The fast reaction between Fe(II) and oxygen[47] favors the heavy isotopes of iron
251 in the resulting Fe(III) minerals that precipitate. Abiotic and biotic Fe(II) oxidation
252 both follow this trend, resulting in ε of ~2-4 ‰ between aqueous Fe(II) and Fe(III)
253 minerals, with minerals enriched in heavy isotopes[17, 18, 29, 31]. Our $\varepsilon^{56}Fe$ for
254 $\delta^{56}Fe(II)_{aq}$ (1.79 to 2.15 ‰ for samples 1 and 2, respectively; **Table 1**), determined
255 from a Rayleigh fit of the $\delta^{56}Fe(II)_{aq}$ data, is on the low end of this range, similar to
256 what was previously documented for Fe(II) oxidation by anoxygenic phototrophs[18,
257 48]. The Rayleigh fit of the $\delta^{56}Fe_{ppt}$ data from both replicates resulted in $\varepsilon^{56}Fe$ of 2.44
258 and 2.98 ‰, larger than that attained for the $\delta^{56}Fe(II)_{aq}$ data (**Table 1**), and within
259 the literature range. Prior explanation for the offset in ε between these two fractions
260 is that following precipitation, the Fe_{ppt} underwent partial equilibration with
261 another phase of iron in the system, possibly a ligand-bound or sorbed Fe(III)

phase[18, 48] or $Fe(II)_{aq}$[29, 49]. Below, we use our mineralogical and microscopic characterizations of the experiment to explore possible exchange processes in this system.

Iron sorption to cells and minerals

The third, quantitatively significant fraction of iron in the system in addition to $Fe(II)_{aq}$ and Fe_{ppt} was Fe_{NaAc} (up to 18% of total Fe). The $\delta^{56}Fe_{NaAc}$ data had an intermediate isotopic composition between $Fe(II)_{aq}$ and Fe_{ppt}, from 0.10 ‰ to -0.73 ‰ throughout the experiment, and contained both Fe(II) and Fe(III) (**Supplementary Table 1**). The presence of Fe(III) in Fe_{NaAc} has previously been observed in Fe(II) oxidation experiments with anoxygenic phototrophs[18], but not with nitrate-dependent Fe(II)-oxidizing bacteria[29]. The Fe_{NaAc} must have been sorbed onto one of the surfaces, either Fe_{ppt} or cells, based on its extraction with sodium acetate[38]. In order to infer whether equilibration processes were occurring between Fe_{NaAc} and Fe_{ppt}, it is necessary to know 1) where Fe_{NaAc} was in our experiments, and 2) what type of iron species [i.e. Fe(II) or Fe(III)] that it was.

Our use of a lectin-binding dye in confocal microscopy documents that EPS was also forming during Fe(II) oxidation with *Synechococcus* PCC 7002 (**Figure 3**). We can use this dataset to first determine whether EPS was important in binding/sorbing iron extracted as Fe_{NaAc}, and then to determine whether iron was associated with the surface of cells and/or Fe_{ppt}. An overlay of **Figures 3a**, **b**, and **c**, which show the location of cells, EPS, and Fe_{ppt} indicates that EPS is co-localized with Fe_{ppt} (**Figure 3d**). The correlation analysis in **Figure 3e** implies there is no

285 spatial overlap of EPS with cells. In previous work with *Synechococcus* PCC 7002
286 under identical growth conditions as in **Figure 3**, a fluorescent sensor for soluble or
287 ligand-bound Fe(III) was used in CLSM, and fluorescence was localized directly at
288 the *Synechococccus* PCC 7002 cell surfaces[18]. While spectral interferences prevented
289 us from simultaneously labeling EPS and Fe(III) in our current CLSM experiments,
290 we can infer from comparing our dataset with the previously published one[34] that
291 there was Fe(III) sorbed to the surface of cells, but not EPS or Fe_{ppt}[50]. In support of
292 this, EPS is expected to stay with the aqueous phase during filtration through a 0.2
293 μm filter[51], or be washed off of Fe_{ppt} in the water wash[18]. We did not detect any
294 Fe(III) in the $Fe(II)_{aq}$ fraction, or measure any detectable iron in the water wash.
295 From these results we exclude EPS as having a major role in binding soluble Fe(III)
296 in the current system. This data indicates that cell surfaces sorbed Fe(III). Previous
297 experiments with *Synechococcus* PCC 7002 cells demonstrated that sorption to cells
298 is a major fate for aqueous iron, although the oxidation state of sorbed iron was not
299 determined in those experiments, so we cannot rule out that some Fe(II) was also
300 sorbed to cells[34]. However, sorption onto cells has previously been documented as a
301 fate for aqueous iron with diverse cyanobacteria, with Fe(III) more commonly
302 detected at the cell surface than Fe(II)[22], via attachment of Fe-O-Fe polymers to
303 phosphoryl groups[22, 23], strengthening the inferences made from CLSM that
304 *Synechococcus* PCC 7002 cells sorbed Fe(III).

305 The other surface in our experiments that could have sorbed iron extracted as
306 Fe_{NaAc} was $Fe_{ppt.}$ The three techniques we used to address mineralogy indicate that
307 our Fe_{ppt} was a mixture of 58% ferrihydrite, 22% goethite, and 20% lepidocrocite

(**Figure 2**), and ferrihydrite was likely the predominant mineral present during the experiments (see **Supplementary Information**). Minerals such as ferrihydrite and goethite, similar to what was present in our experiments, can sorb Fe(II)[27, 52]. Both Fe(II) and Fe(III) were detected in the Fe_{NaAc} (**Supplementary Table 1**), raising the possibility that Fe(III) was extracted from the mineral. However, we verified that no Fe(III) was extracted from synthetic ferrihydrite with our 0.5 M sodium acetate solution prior to beginning experiments (data not shown), consistent with previous reports that used a 1 M sodium acetate solution[38]. Further inference in support of sorbed Fe(II) being extracted from Fe_{ppt} by sodium acetate is that Fe_{ppt} still contained some Fe(II) after extraction, as measured by ferrozine (**Supplementary Table 1**). We take this as evidence that sorbed iron associated with the mineral was predominantly Fe(II), although we cannot exclude that some Fe(III) may also be sorbed to the mineral surface[53, 54].

Fractionation Processes

We observed evidence for three reactions in our experiments that are essential for understanding the observed fractionations of iron isotopes, and these are summarized in **Figure 4.** They are 1) Fe(II) oxidation to Fe(III), which forms $Fe_{ppt,}$ 2) sorption of Fe(III) to cells, and 3) and sorption of Fe(II) to Fe_{ppt}. These observations fit a two step-model of Fe(II) oxidation, where Fe(II) is oxidized and undergoes rapid isotopic equilibration with a pool of Fe(III), which then precipitates as Fe(III) minerals[49]. We suggest, however, that in our experiments, Fe_{ppt} undergoes subsequent partial equilibration with $Fe(II)_{aq}$.

The fitting of our $\delta^{56}Fe(II)_{aq}$ and $\delta^{56}Fe_{ppt}$ with Rayleigh equations representing isolation of the Fe_{ppt} pool from $Fe(II)_{aq}$ after precipitation, and a linear equation representing complete isotopic equilibrium are helpful in interpreting the fractionation mechanisms taking place. The larger ΣX^2 values for linear fits of all data as compared to Rayleigh fits indicates that complete isotopic equilibrium between $Fe(II)_{aq}$ and Fe_{ppt} is not occurring during Fe(II) oxidation and precipitation (**Table 1**). The smaller $\varepsilon^{56}Fe$ values for Rayleigh fits of the $\delta^{56}Fe(II)_{aq}$ (1.79 and 2.15 ‰ as compared to 2.44 and 2.98 ‰ for $\delta^{56}Fe_{ppt}$) are on the order of fractionation observed in other biological Fe(II) oxidation experiments in batch at circumneutral pH: 1.5 ‰[48], 1.5-2 ‰[29], and 1-2 ‰[18]. Such small net fractionations have been noted when the presence of significant quantities of sorbed or ligand-bound Fe(III) has been detected or observed[29].

Up to a few percent of total iron was found as Fe(III) in the Fe_{NaAc} fraction (**Supplementary Table 1**). Based on detection of iron sorbed to cells with a dye that is specific for an aqueous or ligand-bound Fe(III)[42, 43], we suggest that this Fe(III) could equilibrate with $Fe(II)_{aq}$[29, 48]. In experiments with *Synechococcus* sp. cells at pH 6, added Fe(II) [which was adsorbed as Fe(III)] was 1.84 ‰ heavier than aqueous Fe(II)[23], and equilibrium with $Fe(II)_{aq}$ was inferred from the data. This fractionation is very similar to our ε values derived from Rayleigh fits of $\delta^{56}Fe(II)_{aq}$ (1.79 and 2.15 ‰). Because of the similar type of organism that we used, it is likely equilibrium fractionation between $Fe(II)_{aq}$ and Fe(III) sorbed to cells is a relevant process in our experiments.

While the $\delta^{56}Fe_{ppt}$ data are not well fit by a linear model representing complete equilibrium exchange with $Fe(II)_{aq}$, the range of the $\varepsilon^{56}Fe$ determined from Rayleigh fits of the two $\delta^{56}Fe_{ppt}$ datasets (2.44 and 2.98 ‰) are of the same magnitude expected for equilibrium between Fe_{ppt} and $Fe(II)_{aq}$. Wu et al.[31] inferred a $\Delta^{56}Fe_{ferrihydrite\text{-}Fe(II)aq}$ (where $\Delta^{56}Fe_{ferrihydrite\text{-}Fe(II)aq} = \delta^{56}Fe_{ferrihydrite} - \delta^{56}Fe_{Fe(II)aq}$) of 3.2 ‰, while Beard et al. and Frierdich et al. reported a $\Delta^{56}Fe_{goethite\text{-}Fe(II)aq}$ of 1.1 ‰[25, 55]. Considering the 58% ferrihydrite, 22% goethite, and 20% lepidocrocite in our precipitates as determined from X-ray scattering (**Figure 2**), the equilibrium $\Delta^{56}Fe_{Feppt\text{-}Fe(II)aq}$ for our minerals could range from 2.3 to 2.7 ‰, depending on whether the assumed fractionation for lepidocrocite is the same as for goethite or ferrihydrite, respectively. The larger $\varepsilon^{56}Fe$ we calculate for our second dataset (2.98 ‰) may reflect that ferrihydrite, with a larger $\Delta^{56}Fe$ value, was likely the mineral present during active Fe(II) oxidation (see **Supporting Information**).

In our batch experiments, $Fe(II)_{aq}$ may continue to react with Fe_{ppt}, given their proximity and the time frame of experiments (10 days). Sorption of Fe(II) on Fe_{ppt} provides a likely mechanism for partial isotope equilibrium, and is supported by our detection of Fe(II) in Fe_{ppt} (**Supplementary Table 1**). Sorption of Fe(II) is an important pathway in recrystallization of Fe(III) (oxyhydr)oxide minerals, particularly ferrihydrite[28]. During this process, equilibrium atom and electron exchange occur between sorbed Fe(II) and Fe(III) minerals[24], with complete equilibrium attained within two weeks for goethite, for instance[55] (a similar time frame as our 10 day experiment). In this model, Fe(II) sorbs to Fe(III) minerals and donates an electron into the bulk mineral structure, adding to the Fe(III) mineral,

and causing the desorption of a newly produced Fe(II) from the mineral. This is also consistent with the shifts in mineralogy we see during the course of oxidation (see **Supplementary Information).**

We do not see evidence for complete equilibrium between $Fe(II)_{aq}$ and Fe_{ppt}, given the poor linear fit of $\delta^{56}Fe_{ppt}$ (**Table 1**). Atom and electron exchange between Fe_{ppt} and sorbed Fe(II) is expected to be diminished in the presence of organic compounds[30]. Our CLSM data indicate that EPS is co-localized to minerals (**Figure 2**). It is possible that atom and electron exchange can still occur when Fe(III) minerals are co-precipitated with organics, as retardation of this process seems to result from blockage of surface sites when organics coat already formed Fe(III) minerals[52], or if long chain carbon molecules are present[30]. Therefore, we suggest that only partial atom and electron exchange occurred in our system as a result of the EPS coating the Fe_{ppt}.

During atom exchange, the fractionation when $Fe(II)_{aq}$ sorbs onto goethite varies among experiments. One study reports sorbed Fe(II) is 0.73 ‰ heavier than $Fe(II)_{aq}$[56], and another reported sorbed Fe(II) was 1.24 ‰ heavier[25]. Differences are likely due to a lack of equilibrium obtained. Crosby et al.[53, 54] directly measured sorbed Fe(II) extracted with sodium acetate during microbial Fe(III) reduction experiments, which was just 0.3 ‰ heavier than $Fe(II)_{aq}$ for experiments using hematite, and up to 0.8 ‰ heavier for experiments using goethite as the sorbing surface. Our $\Delta^{56}Fe_{FeNaAc\text{-}Fe(II)aq}$ ranged from 0.45 to 2.66 ‰, which is much larger and more variable than the experiments of Crosby et al.[53, 54], which may be in part because our Fe_{NaAc} includes both Fe(II) and Fe(III). Another factor is that in our

399 experiments, the less crystalline mineral ferrihydrite was likely the sorbing surface
400 present during experiments (see **Supplementary Figures 1** and **2** and
401 **Supplementary Information**). Several studies have noted a trend of larger
402 fractionations during sorption to less crystalline minerals or higher surface area
403 minerals[25, 54]. The Fe_{ppt} in our experiments had a surface area of 122.1 $m^2\ g^{-1}$.

404 We calculated $\delta^{56}Fe_{NaAc}$ considering that the Fe(III) fraction of Fe_{NaAc} should be
405 1.84 ‰ heavier that $Fe(II)_{aq}$ due to adsorption of Fe(III) at cell surfaces[23], and the
406 sorbed Fe(II) fraction of Fe_{NaAc} should be at least 0.8 ‰ heavier than $Fe(II)_{aq}$. The
407 calculated $\delta^{56}Fe_{NaAc}$ is a good model of our actual $\delta^{56}Fe_{NaAc}$ values (**Figure 4**). This
408 calculation supports the model presented here, in which Fe(II) is oxidized to Fe(III),
409 which is sorbed onto cells and equilibrates with $Fe(II)_{aq}$, and partial equilibration of
410 $Fe(II)_{aq}$ with Fe_{ppt} via atom and electron exchange is hindered by the presence of
411 EPS on Fe_{ppt}.

412 Our experiments provide evidence that iron isotope fractionation during
413 microbially-influenced Fe(II) oxidation by cyanobacteria is not a simple reaction,
414 controlled only by the abiotic oxidation of Fe(II) with oxygen and rapid precipitation
415 of Fe(III) at circumneutral pH[34]. Multiple secondary processes generate a significant
416 fraction of sorbed iron that is isotopically distinct from either residual $Fe(II)_{aq}$ or
417 Fe_{ppt}, and subsequent equilibration between the iron pools can further modify the
418 isotopic composition of these phases. Our data indicate that sorption of Fe(III) at cell
419 surfaces likely further fractionates the $Fe(II)_{aq}$ pool. In addition, abiotic sorption of
420 Fe(II) to Fe(III) mineral surfaces can also fractionate $Fe(II)_{aq}$, through equilibrium
421 atom and electron exchange subsequent to Fe(II) sorption, despite the presence of

422 EPS. Follow-up experiments could investigate atom and electron exchange in this
423 system. Specifically, isotopically enriched $Fe(II)_{aq}$ solutions mixed with pre-formed
424 cells and minerals would be useful for monitoring atom exchange between the
425 $Fe(II)_{aq}$ and Fe_{ppt}[57].

426 The processes and phases described here can overprint the anticipated
427 fractionations and compositions of Fe(III) minerals and organic-associated iron
428 present in the environment, and can challenge interpretation of the genesis of
429 Fe(III) minerals in the geological record, where the residual $Fe(II)_{aq}$ pool is no
430 longer present[12, 58-60]. Although iron atom and electron exchange has received the
431 most attention as a process relevant to Fe(III)-reducing systems where Fe(II) is in
432 contact with Fe(III) minerals, our data suggest this process could also be relevant in
433 environments where Fe(II) is abundant during Fe(II) oxidation and Fe(III) mineral
434 formation. This includes oxidizing environments with high enough fluxes of Fe(II)
435 for Fe(II) to persist even in the face of rapid oxidation[2, 61], such as Fe(II)-rich springs
436 or seeps, and marine upwelling zones that tap ferruginous bottom waters, past or
437 present[33]. Furthermore, our work documents atom and electron exchange in the
438 presence of iron minerals whose formation pathways are biologically induced, and
439 when organic phases that coat iron minerals. Finally, iron redox cycling and
440 sorption of iron at the surface of cyanobacteria may be an important component of
441 modern and ancient aquatic iron cycling, and our work highlights the effect of such
442 processes on iron isotope systematics.

Acknowledgements

Synechococcus PCC 7002 was a gift of M. Eisenhut. E. Reitter assisted with iron purification and isotope analysis. E. Struve performed the Mastersizer and BET analyses. Portions of this research were carried out at the Stanford Synchrotron Radiation Lightsource (SSRL), a directorate of SLAC National Accelerator Laboratory and an Office of Science User Facility operated by the U.S. Department of Energy Office of Science by Stanford University. R. Davis assisted with EXAFS measurements. The use of the Advanced Photon Source, an Office of Science User Facility operated for the U.S. Department of Energy (DOE) Office of Science by Argonne National Laboratory, was supported by the U.S. DOE under Contract No. DE-AC02-06CH11357. We thank K. Chapman, P. Chupas, and K. Beyer for their support at APS beamline 11-ID-B. E.D.S. was supported by a Carl Zeiss Stiftung Postdoctoral Fellowship, which also supported the work of T.B. W.W. received support from Sino-German (CSC-DAAD) Postdoc Scholarship Program and China Postdoctoral Science Foundation (2014M560115). F.M.M. received support from the Center for Environmental Implications of Nanotechnology (CEINT) funded under NSF cooperative agreement EF-0830093. A.K. was supported by the German Research Foundation (DFG, KA 1736/24-1), and by the European Research Council under the European Union's Seventh Framework Programme (FP/2007–2013)/ERC Grant, Agreement n. 307320 – MICROFOX.

Supporting Information. Supporting methods, discussion, 3 figures and 4 tables.

References

1. Melton, E. D.; Swanner, E. D.; Behrens, S.; Schmidt, C.; Kappler, A., The interplay of microbially mediated and abiotic reactions in the biogeochemical Fe cycle. *Nat Rev Micro* **2014,** *12*, 797-808.
2. Trouwborst, R. E.; Johnston, A.; Koch, G.; Luther III, G. W.; Pierson, B. K., Biogeochemistry of Fe(II) oxidation in a photosynthetic microbial mat: Implications for Precambrian Fe(II) oxidation. *Geochimica et Cosmochimica Acta* **2007,** *71*, 4627-4643.
3. Epping, E. H. G.; Schoemann, V.; de Heij, H., Manganese and Iron Oxidation During Benthic Oxygenic Photosynthesis. *Estuarine, Coastal and Shelf Science* **1998,** *47*, (6), 753-767.
4. Conway, T. M.; John, S. G., Quantification of dissolved iron sources to the North Atlantic Ocean. *Nature* **2014,** *511*, (7508), 212-215.
5. Scholz, F.; McManus, J.; Mix, A. C.; Hensen, C.; Schneider, R. R., The impact of ocean deoxygenation on iron release from continental margin sediments. *Nature Geosci* **2014,** *7*, (6), 433-437.
6. Staubwasser, M.; von Blanckenburg, F.; Schoenberg, R., Iron isotopes in the early marine diagenetic iron cycle. *Geology* **2006,** *34*, (8), 629-632.
7. Severmann, S.; Lyons, T. W.; Anbar, A.; McManus, J.; Gordon, G., Modern iron isotope perspective on the benthic iron shuttle and the redox evolution of ancient oceans. *Geology* **2008,** *36*, (6), 487-490.
8. Stramma, L.; Johnson, G. C.; Sprintall, J.; Mohrholz, V., Expanding Oxygen-Minimum Zones in the Tropical Oceans. *Science* **2008,** *320*, (5876), 655-658.
9. Poulton, S. W.; Canfield, D. E., Ferruginous Conditions: A Dominant Feature of the Ocean through Earth's History. *Elements* **2011,** *7*, (2), 107-112.
10. Canfield, D. E.; Poulton, S. W.; Narbonne, G. M., Late-Neoproterozoic deep-ocean oxygenation and the rise of animal life. *Science* **2007,** *315*, 92-95.
11. Scott, C.; Lyons, T. W.; Bekker, A.; Shen, Y.; Poulton, S. W.; Chu, X.; Anbar, A. D., Tracing the stepwise oxygenation of the Proterozoic ocean. *Nature* **2008,** *452*, (27), 456-459.
12. Czaja, A. D.; Johnson, C. M.; Roden, E. E.; Beard, B. L.; Vogelin, A. R.; Nägler, T. F.; Beukes, N. J.; Wille, M., Evidence for free oxygen in the Neoarchean ocean based on coupled iron-molybdenum isotope fractionation. *Geochimica et Cosmochimica Acta* **2012,** *86*, 118-137.
13. Sahoo, S. K.; Planavsky, N. J.; Kendall, B.; Wang, X.; Shi, X.; Scott, C.; Anbar, A. D.; Lyons, T. W.; Jiang, G., Ocean oxygenation in the wake of the Marinoan glaciation. *Nature* **2012,** *489*, (7417), 546-549.
14. Beard, B. L.; Johnson, C. M.; Cox, L.; Sun, H.; Nealson, K.; Aguilar, C., Iron Isotope Biosignatures. *Science* **1999,** *285*, 1889-1892.
15. Johnson, C. M.; Beard, B. L.; Roden, E. E., The Iron Isotope Fingerprints of Redox and Biogeochemical Cycling in Modern and Ancient Earth. *Annual Review of Earth and Planetary Sciences* **2008,** *36*, (1), 457-493.
16. Schauble, E. A., Applying Stable Isotope Fractionation Theory to New Systems. *Reviews in Mineralogy and Geochemistry* **2004,** *55*, (1), 65-111.

17. Balci, N.; Bullen, T. D.; Witte-Lien, K.; Shanks, W. C.; Motelica, M.; Mandernack, K. W., Iron isotope fractionation during microbially stimulated Fe(II) oxidation and Fe(III) precipitation. *Geochimica et Cosmochimica Acta* **2006,** *70*, 622-639.
18. Swanner, E. D.; Wu, W.; Schoenberg, R.; Byrne, J.; Michel, F. M.; Pan, Y.; Kappler, A., Fractionation of Fe isotopes during Fe(II) oxidation by a marine photoferrotroph is controlled by the formation of organic Fe-complexes and colloidal Fe fractions. *Geochimica et Cosmochimica Acta* **2015,** *165*, (0), 44-61.
19. Kranzler, C.; Lis, H.; Shaked, Y.; Keren, N., The role of reduction in iron uptake processes in a unicellular, planktonic cyanobacterium. *Environ Microbiol* **2011,** *13*, (11), 2990-9.
20. Lis, H.; Kranzler, C.; Keren, N.; Shaked, Y., A Comparative Study of Iron Uptake Rates and Mechanisms amongst Marine and Fresh Water Cyanobacteria: Prevalence of Reductive Iron Uptake. *Life* **2015,** *5*, (1), 841-860.
21. Rose, A. L.; Salmon, T. P.; Lukondeh, T.; Neilan, B. A.; Waite, T. D., Use of superoxide as an Electron Shuttle for Iron Acquisition by the Marine Cyanobacterium *Lyngbya majuscula*. *Environ. Sci. Technol.* **2005,** *39*, 3708-3715.
22. González, A. G.; Pokrovsky, O. S.; Jiménez-Villacorta, F.; Shirokova, L. S.; Santana-Casiano, J. M.; González-Dávila, M.; Emnova, E. E., Iron adsorption onto soil and aquatic bacteria: XAS structural study. *Chemical Geology* **2014,** *372*, (0), 32-45.
23. Mulholland, D. S.; Poitrasson, F.; Shirokova, L. S.; González, A. G.; Pokrovsky, O. S.; Boaventura, G. R.; Vieira, L. C., Iron isotope fractionation during Fe(II) and Fe(III) adsorption on cyanobacteria. *Chemical Geology* **2015,** *400*, (0), 24-33.
24. Williams, A. G. B.; Scherer, M. M., Spectroscopic Evidence for Fe(II)-Fe(III) Electron Transfer at the Iron Oxide-Water Interface. *Environmental Science & Technology* **2004,** *38*, 4782-4790.
25. Beard, B. L.; Handler, R. M.; Scherer, M. M.; Wu, L.; Czaja, A. D.; Heimann, A.; Johnson, C. M., Iron isotope fractionation between aqueous ferrous iron and goethite. *Earth and Planetary Science Letters* **2010,** *295*, (1–2), 241-250.
26. Johnson, C. M.; Roden, E. E.; Welch, S. A.; L., B. B., Experimental constraints on Fe isotope fractionation during magnetite and Fe carbonate formation coupled to dissimilatory hydrous ferric oxide reduction. *Geochimica et Cosmochimica Acta* **2005,** *69*, (4), 963-993.
27. Hansel, C. M.; Benner, S. G.; Neiss, J.; Dohnalkova, A.; Kukkadapu, R. K.; Fendorf, S., Secondary mineralization pathways induced by dissimilatory iron reduction of ferrihydrite under advective flow. *Geochimica et Cosmochimica Acta* **2003,** *67*, (16), 2977-2992.
28. Hansel, C. M.; Benner, S. G.; Nico, P.; Fendorf, S., Structural constraints of ferric (hydr)oxides on dissimilatory iron reduction and the fate of Fe(II). *Geochimica et Cosmochimica Acta* **2004,** *68*, (15), 3217-3229.
29. Kappler, A.; Johnson, C. M.; Crosby, H. A.; Beard, B. L.; Newman, D. K., Evidence for equilibrium iron isotope fractionation by nitrate-reducing iron(II)-oxidizing bacteria. *Geochimica et Cosmochimica Acta* **2010,** *74*, (10), 2826-2842.
30. Pasakarnis, T.; McCormick, M. L.; Parkin, G. F.; Thompson, A.; Scherer, M., FeIIaq-FeIIIoxide electron transfer and Fe exchange - effect of organic carbon. *Environ Chem* **2015,** *12*, 52-63.

555 31. Wu, L.; Beard, B. L.; Roden, E. E.; Johnson, C. M., Stable Iron Isotope
556 Fractionation Between Aqueous Fe(II) and Hydrous Ferric Oxide. *Environmental*
557 *Science & Technology* **2011,** *45*, 1847-1852.
558 32. Reddy, T. R.; Frierdich, A. J.; Beard, B. L.; Johnson, C. M., The effect of pH on
559 stable iron isotope exchange and fractionation between aqueous Fe(II) and goethite.
560 *Chemical Geology* **2015,** *397*, 118-127.
561 33. Swanner, E. D.; Mloszewska, A. M.; Cirpka, O. A.; Schoenberg, R.; Konhauser,
562 K. O.; Kappler, A., Modulation of oxygen production in Archaean oceans by episodes
563 of Fe(II) toxicity. *Nature Geosci* **2015,** *8*, (2), 126-130.
564 34. Swanner, E. D.; Wu, W.; Hao, L.; Wuestner, M.; Obst, M.; Moran, D. M.; McIlvin,
565 M.; Saito, M.; Kappler, A., Physiology, Fe(II) oxidation, and Fe mineral formation by a
566 marine planktonic cyanobacterium grown under ferruginous conditions. *Frontiers in*
567 *Earth Science* **2015,** *3*.
568 35. Wu, W.; Swanner, E. D.; Hao, L.; Zeitvogel, F.; Obst, M.; Pan, Y.; Kappler, A.,
569 Characterization of the physiology and cell-mineral interactions of the marine
570 anoxygenic phototrophic Fe(II)-oxidizer *Rhodovulum iodosum* - implications for
571 Precambrian Fe(II) oxidation. *FEMS Microbiol Ecol* **2014,** *88*, 503-515.
572 36. Llirós, M.; García–Armisen, T.; Darchambeau, F.; Morana, C.; Triadó–Margarit,
573 X.; Inceoğlu, Ö.; Borrego, C. M.; Bouillon, S.; Servais, P.; Borges, A. V.; Descy, J. P.;
574 Canfield, D. E.; Crowe, S. A., Pelagic photoferrotrophy and iron cycling in a modern
575 ferruginous basin. *Scientific Reports* **2015,** *5*, 13803.
576 37. Busigny, V.; Planavsky, N. J.; Jézéquel, D.; Crowe, S.; Louvat, P.; Moureau, J.;
577 Viollier, E.; Lyons, T. W., Iron isotopes in an Archean ocean analogue. *Geochimica et*
578 *Cosmochimica Acta* **2014,** *133*, 443-462.
579 38. Crosby, H.; Johnson, C.; Roden, E.; Beard, B., Coupled Fe(II)-Fe(III) electron
580 and atom exchange as a mechanism for Fe Isotope fractionation during dissimilatory
581 iron oxide reduction. *Environmental Science & Technology* **2005,** *39*, 6698-6704.
582 39. Stookey, L. L., Ferrozine - a new spectrophotometric reagent for iron.
583 *Analytical Chemistry* **1970,** *42*, (7), 779-781.
584 40. Schoenberg, R.; Von Blanckenburg, F., An assessment of the accuracy of stable
585 Fe isotope ratio measurements on samples with organic and inorganic matrices by
586 high-resolution multicollector ICP-MS. *International Journal of Mass Spectrometry*
587 **2005,** *242*, 257-272.
588 41. Moeller, K.; Schoenberg, R.; Grenne, T.; Thorseth, I. H.; Drost, K.; Pedersen, R.
589 B., Comparison of iron isotope variations in modern and Ordovician siliceous Fe
590 oxyhydroxide deposits. *Geochimica et Cosmochimica Acta* **2014,** *126*, (0), 422-440.
591 42. Mao, J.; He, Q.; Liu, W., An rhodamine-based fluorescence probe for iron(III)
592 ion determination in aqueous solution. *Talanta* **2010,** *80*, (5), 2093-2098.
593 43. Mao, J.; Wang, L.; Dou, W.; Tang, X.; Yan, Y.; Liu, W., Tuning the Selectivity of
594 Two Chemosensors to Fe(III) and Cr(III). *Organic Letters* **2007,** *9*, (22), 4567-4570.
595 44. Schmid, G.; Zeitvogel, F.; Hao, L.; Ingino, P.; Floetenmeyer, M.; Stierhof, Y.-D.;
596 Schroeppel, B.; Burkhardt, C.; Kappler, A.; Obst, M., 3D analysis of bacterial cell-
597 (iron)mineral aggregates formed during Fe(II) oxidation by the nitrate-reducting
598 *Acidovorax* sp. strain BoFeN1 using complementary microscopy tomography
599 approaches. *Geobiology* **2014,** *12*, 340-361.

45. Zeitvogel, F.; Schmid, G.; Hao, L.; Ingino, P.; Obst, M., ScatterJ: an ImageJ plugin for the evaluation of analytical microscopy datasets. *Journal of Microscopy* **2014,** *00*, (0), 1-9.
46. Abràmoff, M. D.; Magalhães, P. J.; Ram, S. J., Image processing with IMAGEJ. *Biophotonics Int* **2004,** *11*, 36-42.
47. Stumm, W.; Lee, G. F., Oxygenation of Ferrous Iron. *Industrial and Engineering Chemistry* **1961,** *53*, 143-146.
48. Croal, L. R.; Johnson, C. M.; Beard, B. L.; Newman, D. K., Iron isotope fractionation by Fe(II)-oxidizing photoautotrophic bacteria. *Geochimica et Cosmochimica Acta* **2004,** *68*, (6), 1227-1242.
49. Beard, B.; Johnson, C. M., Fe Isotope Variations in the Modern and Ancient Earth and Other Planetary Bodies. *Reviews in Mineralogy and Geochemistry* **2004,** *55*, 319-357.
50. Hao, L.; Guo, Y.; Byrne, J. M.; Zeitvogel, F.; Schmid, G.; Ingino, P.; Li, J.; Neu, T. R.; Swanner, E. D.; Kappler, A.; Obst, M., Binding of heavy metal ions in aggregates of microbial cells, EPS and biogenic iron minerals measured in-situ using metal- and glycoconjugates-specific fluorophores. *Geochimica et Cosmochimica Acta* **2016,** *180*, 66-96.
51. Bramhachari, P. V.; Dubey, S. K., Isolation and characterization of exopolysaccharide produced by Vibrio harveyi strain VB23. *Letters in Applied Microbiology* **2006,** *43*, (5), 571-577.
52. Jones, A. M.; Collins, R. N.; Rose, J.; Waite, T. D., The effect of silica and natural organic matter on the Fe(II)-catalysed transformation and reactivity of Fe(III) minerals. *Geochimica et Cosmochimica Acta* **2009,** *73*, (15), 4409-4422.
53. Crosby, H. A.; Johnson, C. M.; Roden, E. E.; Beard, B. L., Coupled Fe(II)−Fe(III) Electron and Atom Exchange as a Mechanism for Fe Isotope Fractionation during Dissimilatory Iron Oxide Reduction. *Environmental Science & Technology* **2005,** *39*, (17), 6698-6704.
54. Crosby, H. A.; Roden, E. E.; Johnson, C. M.; Beard, B. L., The mechanisms of iron isotope fractionation produced during dissimilatory Fe (III) reduction by *Shewanella putrefaciens* and *Geobacter sulfurreducens*. *Geobiology* **2007,** *5*, 169-189.
55. Frierdich, A. J.; Beard, B. L.; Reddy, T. R.; Scherer, M. M.; Johnson, C. M., Iron isotope fractionation between aqueous Fe(II) and goethite revisited: New insights based on a multi-direction approach to equilibrium and isotopic exchange rate modification. *Geochimica et Cosmochimica Acta* **2014,** *139*, 383-398.
56. Mikutta, C.; Wiederhold, J. G.; Cirpka, O. A.; Hofstetter, T. B.; Bourdon, B.; Von Gunten, U., Iron isotope fractionation and atom exchange during sorption of ferrous iron to mineral surfaces. *Geochimica et Cosmochimica Acta* **2009,** *73*, 1795-1812.
57. Welch, S. A.; Beard, B. L.; Johnson, C. M.; Braterman, P. S., Kinetic and equilibrium Fe isotope fractionation between aqueous Fe(II) and Fe(III). *Geochimica et Cosmochimica Acta* **2003,** *67*, (22), 4231-4250.
58. Planavsky, N.; Rouxel, O. J.; Bekker, A.; Hofmann, A.; Little, C. T. S.; Lyons, T. W., Iron isotope composition of some Archean and Proterozoic iron formations. *Geochimica et Cosmochimica Acta* **2012,** *80*, (0), 158-169.

644 59. Johnson, C. M.; Beard, B. L.; Klein, C.; Beukes, N. J.; Roden, E. E., Iron isotopes
645 constrain biologic and abiologic processes in banded iron formation genesis.
646 *Geochimica et Cosmochimica Acta* **2008,** *72*, (1), 151-169.
647 60. Rouxel, O. J.; Bekker, A.; Edwards, K. J., Iron Isotope Constraints on the
648 Archean and Paleoproterozoic Ocean Redox State. *Science* **2005,** *307*, (5712), 1088-
649 1091.
650 61. Wu, L.; Brucker, R. P.; Beard, B. L.; Roden, E. E.; Johnson, C. M., Iron isotope
651 characteristics of hot springs at Chocolate Pots, Yellowstone National Park.
652 *Astrobiology* **2013,** *13*, (11), 1091-1101.
653

Figure Captions:

Figure 1. a. Sample 1 and b. sample 2 are biological replicates of the Fe(II) oxidation experiment with *Synechococcus* PCC 7002. Green circles are $\delta^{56}Fe(II)_{aq}$ data, orange squares are $\delta^{56}Fe_{ppt}$ data, and blue diamonds are $\delta^{56}Fe_{NaAc}$ data. The solid green lines are the Rayleigh fits of the $\delta^{56}Fe(II)_{aq}$ data, with an $\varepsilon^{56}Fe$ for $Fe(II)_{aq}$ of 1.79 ‰ (panel a) to 2.15 ‰ (panel b). The solid orange lines are the Rayleigh fits of the $\delta^{56}Fe_{ppt}$ data, with $\varepsilon^{56}Fe$ for $\delta^{56}Fe_{ppt}$ of 2.44 ‰ (panel a) and 2.98 ‰ (panel b). The linear fits are shown as dotted lines for reference.

Figure 2. a. X-ray diffraction (XRD) pattern obtained from X-ray total scattering data of the Fe_{ppt} phase after complete Fe(II) oxidation, freeze-drying, and water washing. The indexed reflections for lepidocrocite (Lp) and goethite (Gt) are shown. b. A 3-component linear combination fit of 58% ferrihydrite, 22% goethite, and 20% lepidocrocite (**Supplementary Table 4**).

Figure 3. CLSM images of *Synechococcus* PCC 7002 cultured anoxically with 4.5 mM Fe(II). a. Autofluorescent cells, b. stained with the lectin-binding dye SBA-488, c. the reflection signal from Fe(III) minerals, and d. an overlay of a, b, and c. Correlation plot of the fluorescence intensity in individual pixels from e. autofluorescence (a) vs. SBA-488 (b), and f. SBA-488 (b) vs. Fe(III) minerals (c). This analysis demonstrates that EPS, which is bound by SBA-488, is coating Fe(III) minerals, but is not spatially associated with cells.

677

678 **Figure 4.** The controls on the overall iron isotope fractionation in the system are 1)
679 Fe(II) oxidation and precipitation of Fe(III) as Fe_{ppt}; 2) sorption of Fe(III) to cells;
680 and 3) equilibrium atom and electron exchange after sorption of $Fe(II)_{aq}$ to Fe_{ppt}. 1
681 generates Fe_{ppt} (dashed orange line) that is 2-3 ‰ heavier than $Fe(II)_{aq}$ (solid green
682 line). 2 produces sorbed Fe(III) on cells with an estimated equilibrium $\Delta^{56}Fe_{FeNaAc-Fe(II)aq}$
683 of 1.84 ‰[23]. 3 produces Fe(II) sorbed on goethite with an estimated
684 $\Delta^{56}Fe_{FeNaAc-Fe(II)aq}$ of 0.8 ‰[54]. The resulting $\delta^{56}Fe_{NaAc}$ predicted from 2 and 3 are
685 denoted by the light blue diamonds.

686

687

688

689

690

691

692

693

694

695

696

697

698

699

Table 1. Iron isotope data from experiments with *Synechococcus* PCC 7002. Each sample was measured twice.

Replicate	Sample	Fraction of Fe(II) oxidized	$\delta^{56}Fe_{aq}$(‰)	2SE	$\delta^{56}Fe_{ppt}$ (‰)	2SE	$\delta^{56}Fe_{NaAc}$ (‰)	2SE
Sample 1	A1	0.00	0.13	0.05	ND		ND	
	B1	0.42	-0.34	0.03	ND		0.10	0.08
	D1	0.36	-0.97	0.04	2.16	0.04	ND	
	E1	0.43	-1.22	0.04	1.96	0.03	-0.36	0.04
	F1	0.49	-1.49	0.04	1.87	0.04	-0.65	0.04
	G1	0.57	-1.75	0.05	1.74	0.03	ND	
	H1	0.60	-2.05	0.04	1.55	0.03	-0.42	0.05
	I1	0.72	-2.53	0.05	1.25	0.03	-0.73	0.04
	J1	0.81	-3.25	0.05	0.97	0.04	-0.59	0.04
	K1	0.99	ND		0.10	0.04	ND	
Rayleigh fit		ε	2.15		2.44		NA	
		ΣX^2	0.66		0.06			
Linear fit		ε	2.90		3.42		NA	
		ΣX^2	0.85		0.38			
Sample 2	A2	0	-0.08	0.04	ND		ND	
	B2	0.47	-0.57	0.05	ND		*-11.11	0.06
	D2	0.41	-1.08	0.04	2.07	0.04	-0.33	0.06
	E2	0.48	*-8.75	0.07	1.97	0.03	-0.31	0.04
	G2	0.57	-1.59	0.04	1.83	0.04	-0.18	0.04
	H2	0.56	-1.75	0.05	1.75	0.04	-0.09	0.04
	I2	0.65	-1.96	0.04	1.59	0.03	-0.57	0.04
	J2	0.63	-2.04	0.04	1.58	0.04	ND	
	K2	0.99	ND		0.07	0.03	ND	
Rayleigh fit		ε	1.79		2.98		NA	
		ΣX^2	0.47		0.36			
Linear fit		ε	2.66		4.17		NA	
		ΣX^2	0.84		1.23			

ND = not determined, due to a low amount of sample. NA = not applicable. *Samples from B2 and E2 had anomalous values for $\delta^{56}Fe_{NaAc}$ and $\delta^{56}Fe_{aq}$, respectively. These samples were most likely lost after drying down due to electrostatic charging of the Teflon beakers. These results are therefore excluded from further analysis.

700

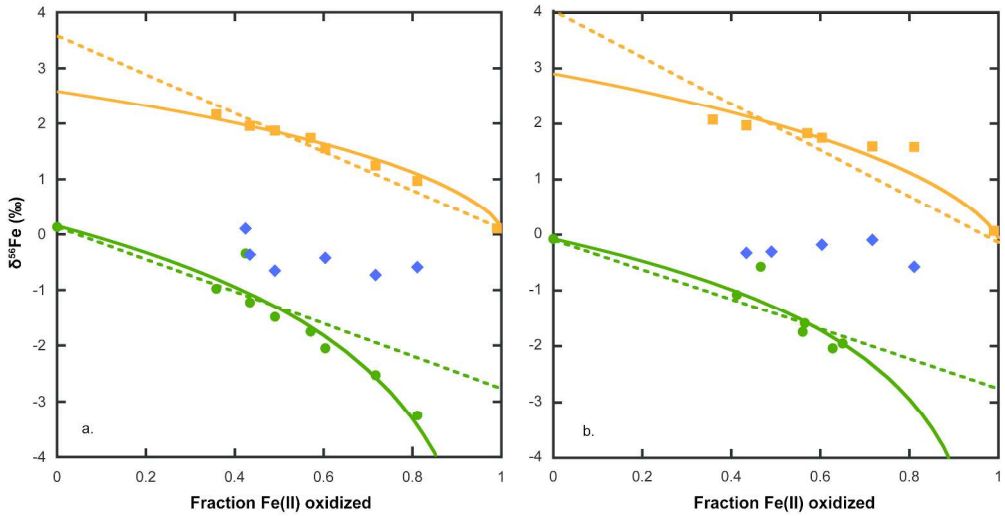

Figure 1. a. Sample 1 and b. sample 2 are biological replicates of the Fe(II) oxidation experiment with Synechococcus PCC 7002. Green circles are δ56Fe(II)aq data, orange squares are δ56Feppt data, and blue diamonds are δ56FeNaAc data. The solid green lines are the Rayleigh fits of the δ56Fe(II)aq data, with an ε56Fe for Fe(II)aq of 1.79 ‰ (panel a) to 2.15 ‰ (panel b). The solid orange lines are the Rayleigh fits of the δ56Feppt data, with ε56Fe for δ56Feppt of 2.44 ‰ (panel a) and 2.98 ‰ (panel b). The linear fits are shown as dotted lines for reference.

275x140mm (300 x 300 DPI)

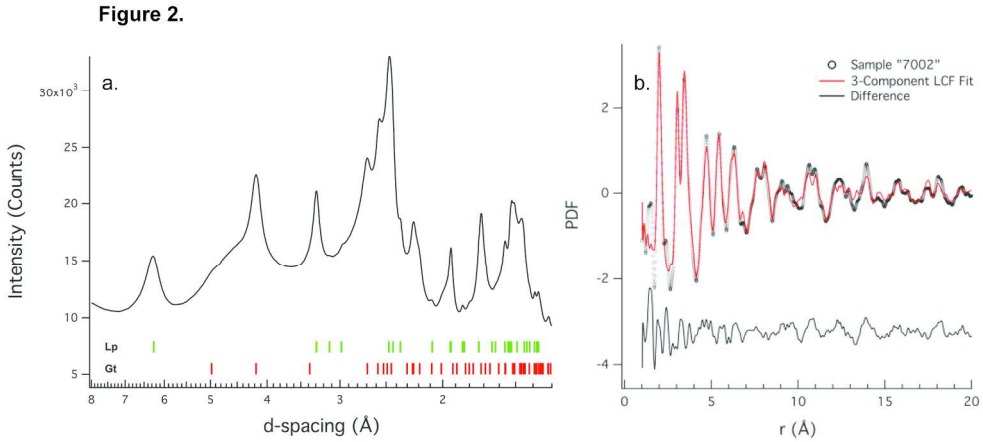

Figure 2. a. X-ray diffraction (XRD) pattern obtained from X-ray total scattering data of the Feppt phase after complete Fe(II) oxidation, freeze-drying, and water washing. The indexed reflections for lepidocrocite (Lp) and goethite (Gt) are shown. b. A 3-component linear combination fit of 58% ferrihydrite, 22% goethite, and 20% lepidocrocite (Supplementary Table 4).

205x89mm (300 x 300 DPI)

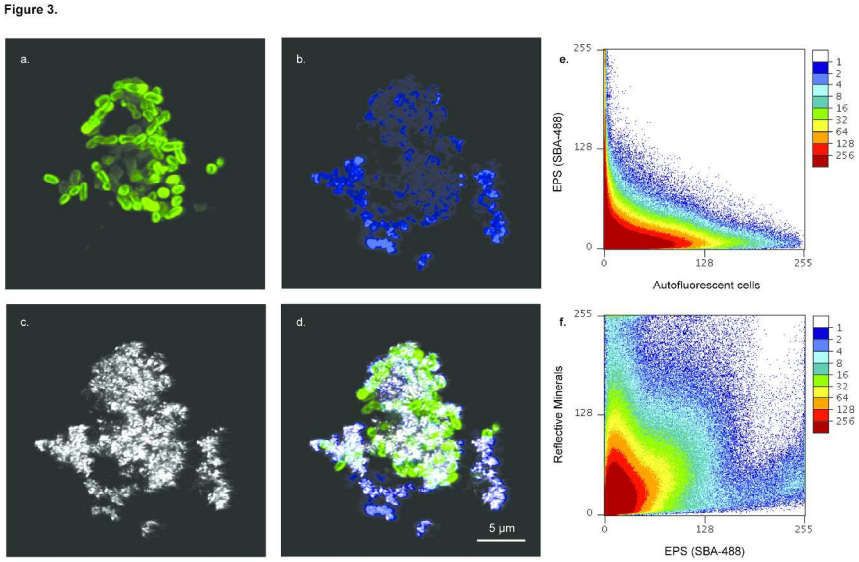

Figure 3. CLSM images of Synechococcus PCC 7002 cultured anoxically with 4.5 mM Fe(II). a. Autofluorescent cells, b. stained with the lectin-binding dye SBA-488, c. the reflection signal from Fe(III) minerals, and d. an overlay of a, b, and c. Correlation plot of the fluorescence intensity in individual pixels from e. autofluorescence (a) vs. SBA-488 (b), and f. SBA-488 (b) vs. Fe(III) minerals (c). This analysis demonstrates that EPS, which is bound by SBA-488, is coating Fe(III) minerals, but is not spatially associated with cells.

329x203mm (300 x 300 DPI)

Figure 4.

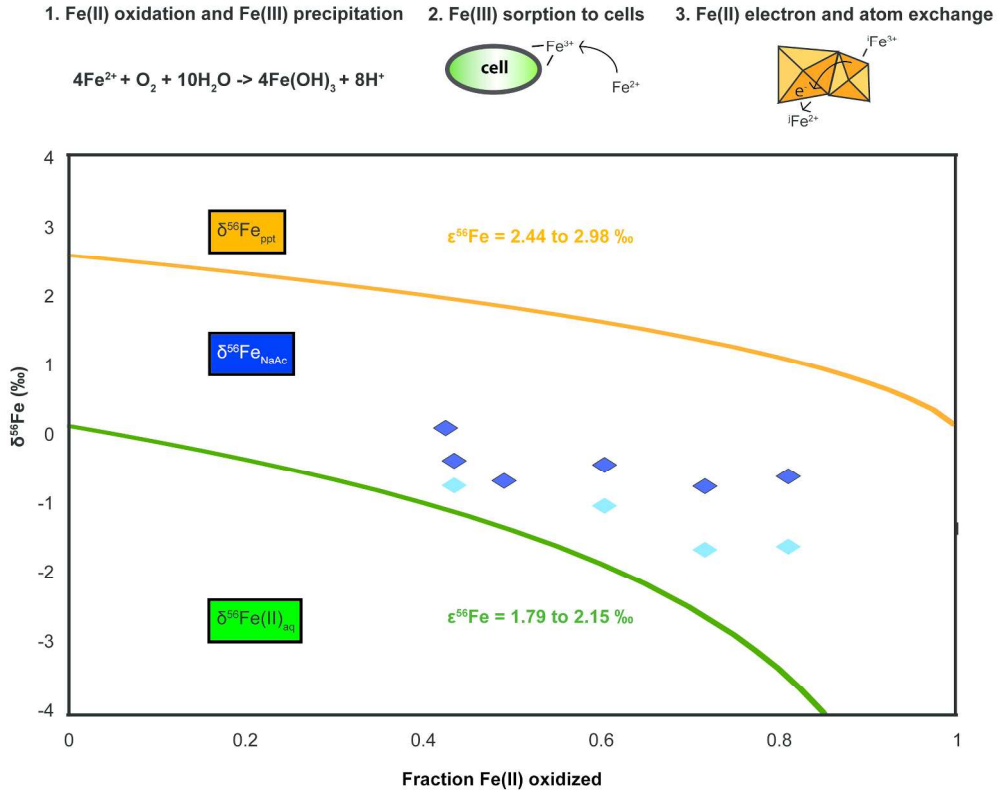

Figure 4. The controls on the overall iron isotope fractionation in the system are 1) Fe(II) oxidation and precipitation of Fe(III) as Feppt; 2) sorption of Fe(III) to cells; and 3) equilibrium atom and electron exchange after sorption of Fe(II)aq to Feppt. 1 generates Feppt (dashed orange line) that is 2-3 ‰ heavier than Fe(II)aq (solid green line). 2 produces sorbed Fe(III) on cells with an estimated equilibrium Δ56FeFeNaAc-Fe(II)aq of 1.84 ‰23. 3 produces Fe(II) sorbed on goethite with an estimated Δ56FeFeNaAc-Fe(II)aq of 0.8 ‰54. The resulting δ56FeNaAc predicted from 2 and 3 are denoted by the light blue diamonds.

230x197mm (300 x 300 DPI)

TOC Art

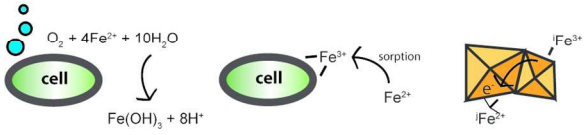

TOC art

141x128mm (300 x 300 DPI)